J Seismol (2009) 13:241–252
DOI 10.1007/s10950-008-9124-0

ORIGINAL ARTICLE

Construction of regional and local seismic anisotropic structures from wide-angle seismic data: crustal deformation in the southeast of China

Z. Zhang · J. Teng · J. Badal · E. Liu

Received: 19 June 2007 / Accepted: 4 February 2008 / Published online: 4 September 2008

Abstract We present a method to obtain spatial distributions of seismic anisotropy associated with regional stress and local faulting in the crust from wide-angle seismic data. The method contains three steps. The first step consists of obtaining radial- and transverse-component seismic sections using a pre-stack depth migration algorithm from the S-wave velocity model determined by conventional interpretation of picked intra-crustal seismic events. In the second step, we compute time delays between split shear-waves and polarizations of fast split shear-waves by minimizing the transverse-component seismic energy. The time delay and polarization in each layer are derived using a layer-stripping method. The final step is to estimate the average splitting parameters along the whole profile. Thus, the average time delay and polarization can be regarded as caused by the effects owing to regional structure and stress fields, whereas the residual values of the splitting parameters are considered to be related to local structures and local faulting. Our method allows us to construct multi-layer anisotropic images, which may later be interpreted in terms of intra-layer coupling/decoupling or deformation. We present results from a set of three-component seismic data acquired by a controlled source experiment in the southeast region of China. The results demonstrate that the average polarizations and time delays are consistent with the direction and strength of the stress field, and their lateral variations related to local anisotropy match the spatial distribution of surface faulting crossing the acquisition seismic profile.

Keywords The Yangtze block · The Cathaysia block · Wide-angle seismic data · Seismic anisotropy · Regional stress · Local faulting

Z. Zhang (✉) · J. Teng
State Key Laboratory of Lithosphere Evolution,
Institute of Geology and Geophysics,
Chinese Academy of Sciences,
Beijing 100029, China
e-mail: zhangzj@mail.iggcas.ac.cn

J. Badal
Physics of the Earth, Sciences B,
University of Zaragoza, Pedro Cerbuna 12,
50009 Zaragoza, Spain
e-mail: badal@unizar.es

E. Liu
Formerly British Geological Survey, West Mains Road, Edinburgh EH9 3LA, UK

Present Address:
E. Liu
ExxonMobil URC, Houston, TX, USA

1 Introduction

Many recent studies have shown that seismic anisotropy may be used to uncover structures and evolution of the earth's crust and upper mantle

as it is closely related to the strain-induced preferentially oriented anisotropic minerals (Mooney and Brocher 1987; Christensen and Mooney 1995; Savage 1999). The polarizations of fast split shear-waves and time delays between the fast and slow split shear-waves, are used to infer the orientation of the principal axes of strain and the thickness of anisotropic layers in the upper mantle (Silver and Chan 1991; Savage 1999; Kendall 2000; Vecsey et al. 2007), and to detect the present and past tectonic activities in several mountainous regions (Vinnik et al. 1989), even to study plate motions and global convection (Babuska and Cara 1991). In these studies, the anisotropic effects due to local faulting, which may show seismic signature of tectonic activities, have been neglected or have large uncertainties associated with the measurements of polarization directions and time delays. To reveal anisotropic effects due to local faulting, three-component seismic data recorded by densely distributed seismic stations have been analyzed. Shear-wave reflection data from a wide-angle seismic experiment provide valuable information about the effects of local faulting and crust-scale deformation. Generally, reflections within the time window constrained by the reflection events from the crystalline basement and the Moho can meet the requirement of the shear-wave window (Booth and Crampin 1985; Liu and Crampin 1990) even though the signal/noise ratio may not be very high. This is also an accepted assumption when radial- and transverse-component shear-wave records (at the surface) are used to directly detect shear-wave splitting (Carbonell and Smithson 1991; Godfrey et al. 2000; Zhang et al. 2000a). In all the previous studies, shear-wave splitting measurements are undertaken in the space–time domain, and therefore it is difficult to obtain depth-dependent anisotropic parameters.

In the last decade, the pre-stack depth migration (PSDM) method has been used to study crustal structures using wide-angle seismic data (Lafond and Levander 1995; Zhang et al. 2000a; Morozov and Levander 2002). The PSDM originates from exploration seismics. For crustal studies, the fold number from wide-angle seismic experiments may not be as high as used in conventional 3D industry-type seismic reflection surveys.

In this paper, we present a scheme to image the spatial distribution of anisotropic parameters in the crust from wide-angle seismic data. By estimating splitting parameters along the whole profile or tectonic blocks crossed by the wide-angle seismic sounding, the average time delays and polarization can be obtained and are interpreted as due to regional anisotropy (regional stress), whereas the residual values of the splitting parameters are thought to be related to local anisotropy (local faulting).

2 Test of pre-stack depth migration on synthetic data

We utilize synthetic shear-wave data to illuminate the scheme to image the spatial distribution of shear-wave splitting parameters in the crust from wide-angle seismic data. Three-component seismic data are generated using a finite-difference algorithm (Zhang et al. 2000b; Yang et al. 2002). Figure 1a presents a geological model with three layers, where the top layer is anisotropic and the second and the bottom layers are isotropic. The parameters of the anisotropic medium are Vp = 4.2 km/s, Vs = 2.94 km/s, $\rho = 2.6$ g/cm^3, and crack density $\varepsilon = 2\%$ and the survey line is at azimuth = 0° relative to the strikes of vertically aligned cracks for the medium 1 (Fig. 1a), representing the background anisotropy, which can be considered as due to horizontal regional stress. In order to describe the influences of local faults, we assume there are two faults in the background medium: one fault penetrates to the bottom of the first layer, and another fault penetrates to the bottom of the second layer. The related parameters to describe the faults are Vp = 4.1 km/s, Vs = 2.87 km/s, ρ = 2.55 g/cm^3, ε = 4% and the survey line azimuth = 30° relative to the strikes of vertically aligned cracks for the first shallow fault (F1 in Fig. 1a); and Vp = 4.533 km/s, Vs = 3.096 km/s, ρ = 2.8 g/cm^3, ε = 4%, and the azimuth = 30° relative to the strikes of vertically aligned cracks for the deep fault (F2 in Fig. 1a). Media 2 and 3 are both isotropic with Vp = 4.8 km/s, Vs = 3.36 km/s, $\rho = 3.0$ g/cm^3 for medium 2 and Vp = 5.0 km/s, Vs=3.0 km/s, ρ=3.2 g/cm^3 for medium 3. The model size *nx* by *nz* is 1,001 by 81 and the

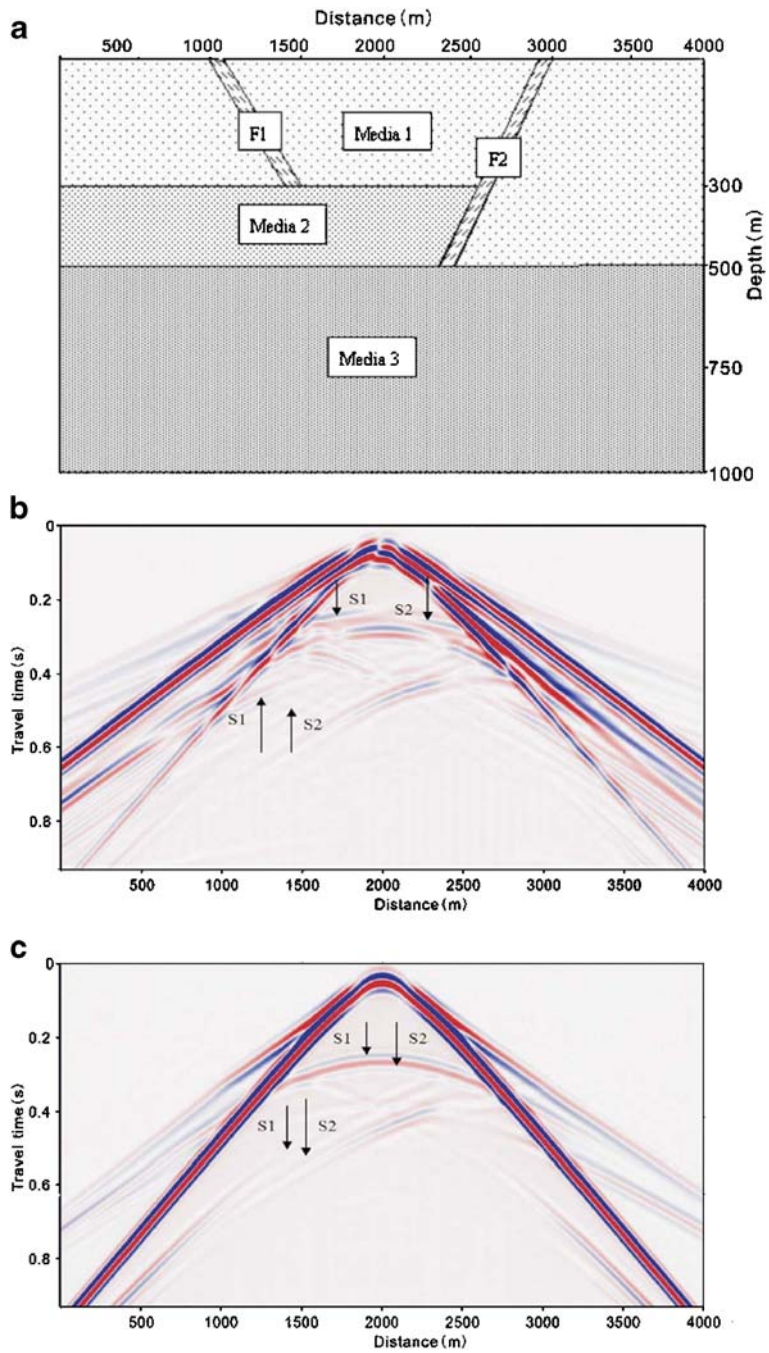

Fig. 1 **a** Geological model with three layers: the top layer (*Medium 1*) is anisotropic and the other two layers (*Media 2* and *3*) are isotropic. There are two faults on the background of the transverse isotropic medium: one fault (*F1*) penetrates to the bottom of the first layer, and another fault (*F2*) penetrates to the bottom of the second layer. Synthetic **b** radial- and **c** transverse-component seismic gathers. The fast and slow split shear-waves from the upper and lower layer are denoted by *S*1 and *S*2, respectively

grid spacing is 5 m. The time sampling rate is 2 ms and the Ricker wavelet with a dominant frequency of 35 Hz is used. Figure 1b and c show the radial- and transverse-component seismic gathers for the shot on the surface location at (701, 1). The fast and slow split shear-waves from the upper and lower layer are denoted by S1 and S2, respectively. From the radial- and transverse-components, we can construct the spatial distribution of shear-wave splitting parameters using the following three steps.

In the first step, we obtain radial- and transverse-component reflectivity sections using a pre-stack depth migration from the S-wave ve-

locity model determined from conventional interpretation of picked intra-crustal seismic events. Figure 2a and b present the radial- and transverse-component reflectivity images after pre-stack depth migration from the S-wave crustal velocity model (Fig. 1a).

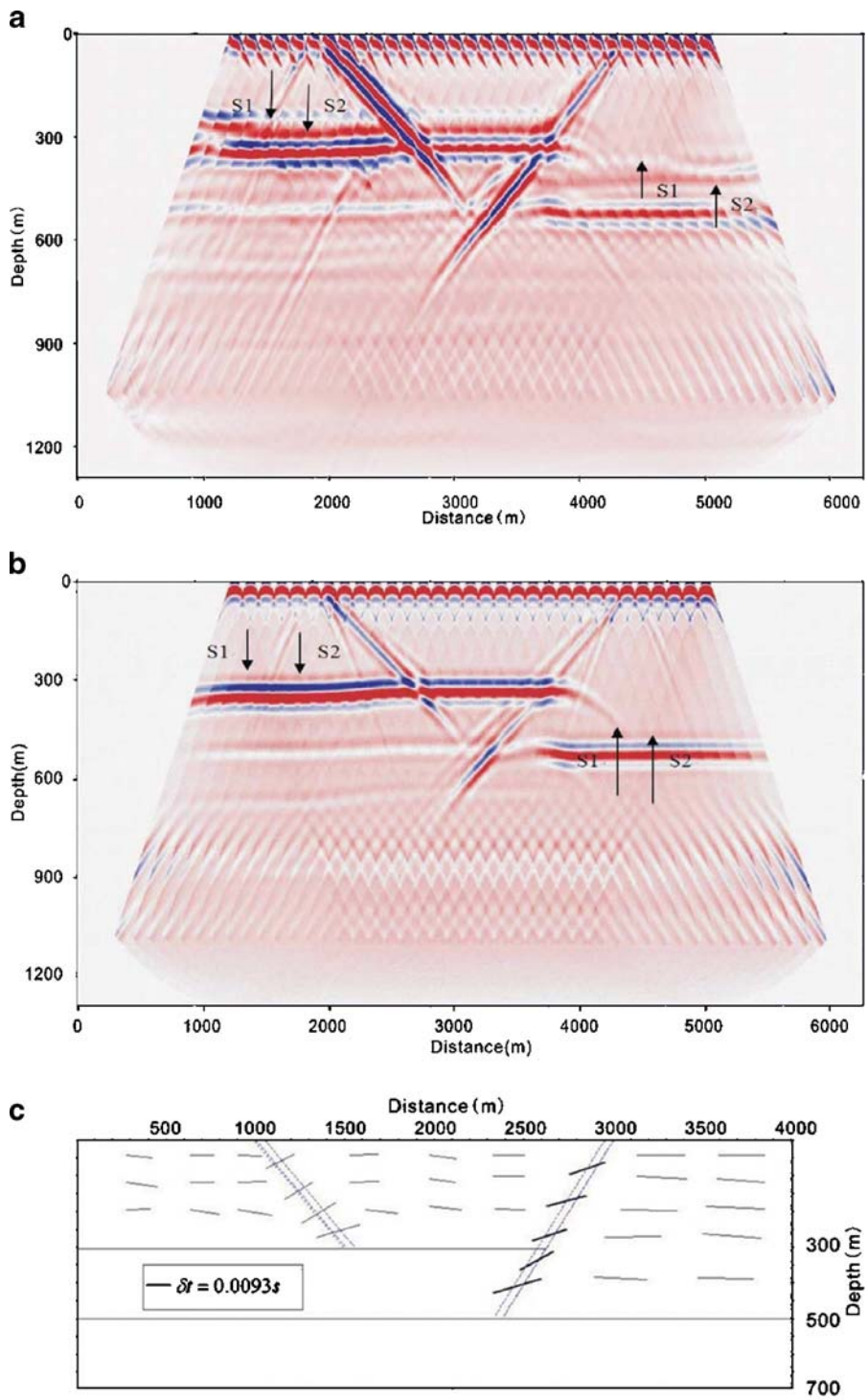

Fig. 2 **a** Radial- and **b** transverse-component seismic reflectivity images obtained from the pre-stack depth migration using the velocity model given in Fig. 1a and seismic data in Fig. 1b and c. **c** Shear-wave splitting image (time delays and fast split wave polarizations) derived from the previous seismic reflectivity sections

The second step is to compute time delays between split shear-waves and polarizations of fast split shear-waves by minimizing the transverse-component seismic energy from the previous reflectivity sections (Fig. 2c). The time delay and polarization in each layer are derived from a layer-stripping approach (Vinnik et al. 1989; Silver and Chan 1991; Savage 1999; Teanby and Kendall 2004; Crampin and Gao 2006). All these computation procedures to estimate time delays and polarizations are implemented in time domain. After the conversion of pre-stack migrated data from depth section into time section with a shear-wave velocity model, the estimation of time delays between split shear-waves and polarizations of fast split shear-waves and layer stripping can be realized in the same way as in PS converted-wave (radial- and transverse-component) sections. In principle, the processing method needs to take account of the variation in splitting parameters with ray geometry and path length, which can only be realized after we obtain an accurate anisotropic model for migration. Obviously, neglecting the dependence of splitting parameters with ray geometry and path length in post- and pre-stack migration will lead to some uncertainties in splitting parameters for cracked/fractured reservoir description and tectonic deformation study.

Finally, we estimate the average splitting parameters along the whole profile (this average is similar to the calculation of the regional stress field from numerous stress measurements), and the residuals are considered to be related to the local stress field. Thus, the average time delays and polarizations are viewed as the effects caused by regional anisotropy (Fig. 3a), whereas the residual values of the splitting parameters are interpreted as due to local anisotropy (Fig. 3b). From Fig. 3, we can see the polarizations at regional scale are consistent with the regional stress, and the polarizations associated with local anisotropy correspond to local features. This method can thus be used to construct anisotropic images for multi-layers.

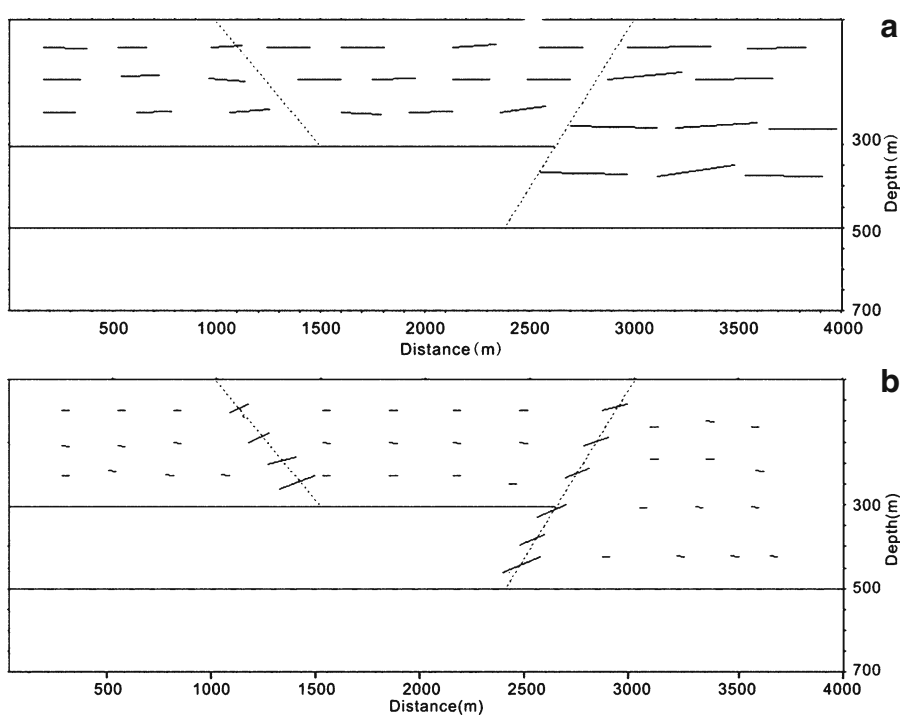

Fig. 3 Regional (**a**) and local (**b**) anisotropy images from shear-wave splitting after a layer-stripping approach with radial- and transverse-component seismic data (Fig. 2a and b)

3 Application to real data acquired in the southeast of China

Understanding the tectonic evolution of southeastern China is among one of the most exciting problems in modern earth science regarding the occurrence of the collision and transition of various cratons during the Precambrian period (Huang 1977), Paleozoic (Zhang et al. 1984) and Mesozoic (Hsu and Sun 1988; Hsu and Li 1990; Gilder and Coe 1993, 1995; Gilder et al. 1996; Chen and John 1998; Zhou and Li 2000). The lateral offset of marker beds of the order of hundreds of kilometers and the identification of major shear zones have prompted to suggest that the entire eastern part of the Chinese landmass was dominated by the Mesozoic Sinistral shear system (Xu et al. 1987; Pei and Hong 1995; Hong et al. 1990, 2002). Hsu and Sun (1988) and Hsu and Li (1990) claimed that a series of fold belts within the region and the southeast of the Yangtze block were accreted by the subduction and the closure of ocean basins in Alpine-type collisions to the Yangtze block in the early Mesozoic or later. As the lithosphere experienced a strong deformation due to the collision of the Yangtze and the Cathaysia blocks, the above two contradictory views may be unraveled by the study of the crustal-scale seismic anisotropy structure beneath the area.

We analyze the three-component wide-angle seismic data acquired in the southeast of China with a focus on seismic anisotropy to investigate the crustal deformation in order to evaluate the two contradictory views about the tectonics of the Yangtze and the Cathaysia blocks.

3.1 Wide-angle seismic data and velocity structure

The three-component wide-angle seismic data were acquired by five in-line active sources in

Fig. 4 Simplified structure map of the southeast of China and neighbor areas showing the wide-angle seismic profile Tunxi–Wenzhou. The *inset in the lower left corner* indicates the location of the study area (*shaded zone*) with respect to the rest of continental China. Up to 85 portable seismic stations (*triangles*) were installed and five shots were fired at different sites (*stars*): Fengle, Xinanjiang, Songyang, Qingtian and Dongtou. The major active faults and basins crossed by the long linear antenna are: (*1*) Lin'an–Majin, (*2*) Wuxing–Jiande, (*3*) Qiuchuan–Xiaoshan, (*4*) Jiangshan–Shaoxing, (*5*) Quzhou–Tangxian, (*6*) Shangyu–Lishui, (*7*) Lishui–Yuyao (*8*) Ningbo–Longquan, (*9*) Zhenhai–Wenzhou, (*I*) Jinqu Basin, (*II*) Bihu Basin, Songyang Plain, (*III*) Wenzhou–Pinyang Hollow, Wenping Depression

1990 (see Fig. 4). The P- and S-wave traveltime interpretations are described in detail elsewhere (Xiong et al. 1993; Zhang et al. 2005). In this study, we firstly rotate the shear-wave data from the North–South (NS) and the East–West (EW) directions to the radial and transverse components, and then obtain the reduced shot-gather shear-wave sections for the radial and transverse components with a reduction of shear-wave velocity of 3.5 km/s. An example of receiver gathers with the shot at Fengle is displayed in Fig. 5, where the top seismic gather is the radial component and the lower section is the transverse component. We can see that in general the data are of very high quality. The interpreted events are shear-wave refractions from the boundary between crust and the uppermost part of the upper mantle or the Moho (Sn), and shear-wave reflections from within the upper to the lower crust (S1, S2, S3 and S4) and the Moho (SmS). In the following pre-stack migration the refraction waves are excluded in order to satisfy the shear-wave window requirement. The P-wave velocity model is interpreted based on the traveltimes of the Pg, Pn, PmP arrivals and other arrivals within the crust (Xiong et al. 1993; Zhang et al. 2005). In the interpretation of crustal shear-wave velocity structure, we fix the reflector geometries in the crust as determined from the P-wave velocity structure inverted from P-wave data, and adjust shear-wave velocities to fit the observed shear-wave traveltime. The final crustal shear-wave velocity model is shown in Fig. 6a.

To study the shear-wave arrivals from the crust, we use the pre-stack depth migration (Zhang et al. 2000b) to reconstruct the radial- and transverse component shear-wave reflection images in the crust from the five shot wide-angle seismic data. From the ray coverage of the experiment, we know that the maximum coverage is five in the central portion of the profile, and most of the portions of the crust are stacked by three times (Zhang et al. 2005). So even though the fold is not as high as in seismic data used in hydrocarbon

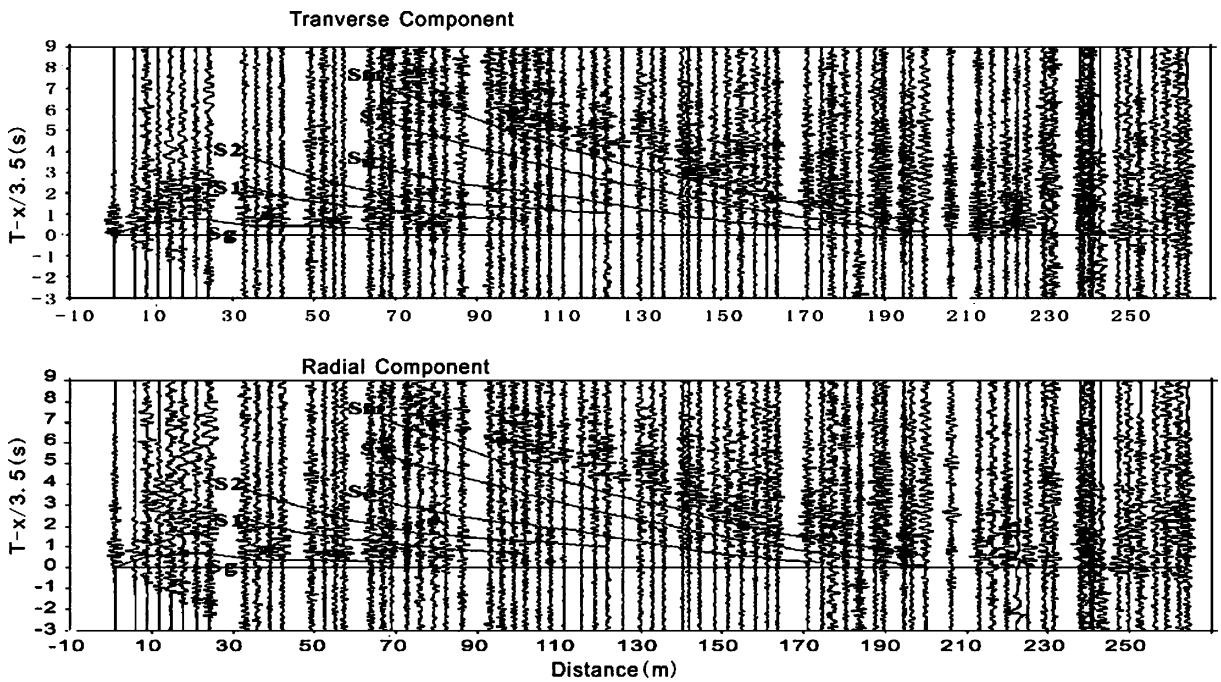

Fig. 5 Shot-common record sections of the transverse (**a**) and radial (**b**) components of the S-wave motion recorded from the shot fired at Fengle Reservoir, near Tunxi, Anhui Province (Fig. 4). The rest of shots fired at Xinanjian, Songyang, Qingtian and Dongtou, Zhejiang Province, provided similar record sections. Each section shows S-phases and is presented at reduced time scale (with a reduction velocity of 3.5 km/s)

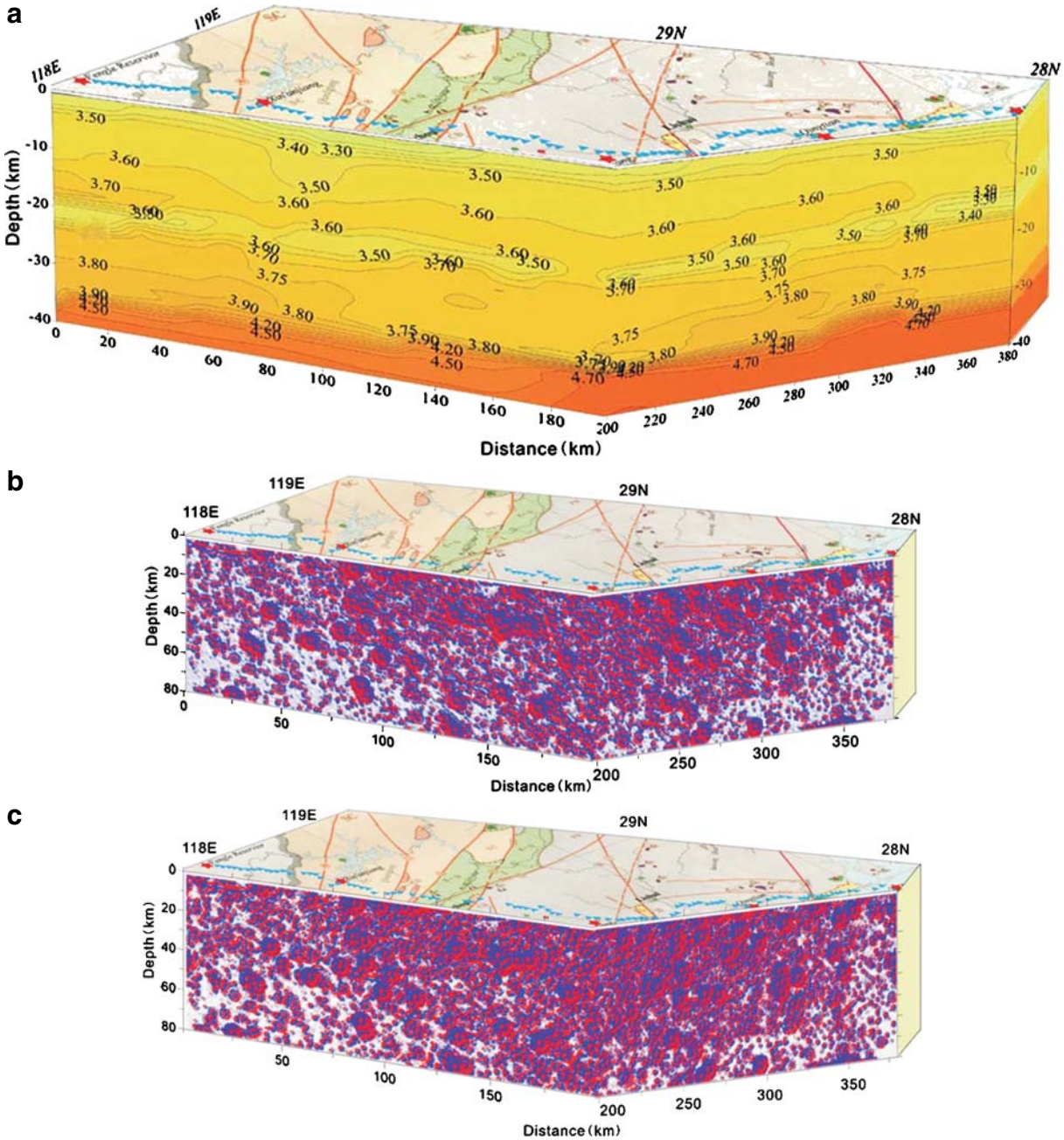

Fig. 6 S-wave velocity model for southeastern China (**a**) showing an overall view of the upper crust, middle crust, lower crust, Moho discontinuity and lithospheric mantle. Velocities are given in km/s. Reflection images after shear-wave pre-stack depth migration of the wide-angle seismic data for **b** radial- and **c** transverse-component, respectively. Traces of major active faults (Fig. 5) have been drawn on top of the three plots in order to provide a comprehensible view

industry (Mooney and Brocher 1987), we may still determine the reflection pattern using the same migration scheme to that used in conventional seismic data. In the migration of wide-angle seismic data, we use the final interpretation of shear-wave velocity as the input model, and set the depth and horizontal intervals to be 0.5 km. Figure 6b and c show the shear-wave reflection sections for the radial and transverse components, respectively. From these figures and crustal P-, S-wave velocity models, we can see that there are at least two shear-waves with strong amplitudes, one at the depth of approximately 20 km, and another from the Moho discontinuity (about 35 km).

3.2 Local anisotropy

After we have obtained the shear-wave images in the depth domain for the radial and transverse components (Fig. 6b and c), we estimate the polarizations of fast split shear-waves and the time delays between split shear-waves using the technique of Silver and Chan (1991), which is applicable to time series data. We transform the shear-wave reflection sections from depth domain into time domain, and estimate fast shear-wave polarization and time delays in the time domain, and finally transform the data back into depth domain. Since the results are averaged over the depth, a layer-stripping technique to eliminate the effects of the underlying layers is used (Vinnik et al. 1989).

From the procedure described above, we can obtain the final images of anisotropy. Figure 7 shows the final results for the residual polarizations of the fast shear-waves derived from shear-wave splitting analysis. In this and following sections we discuss residual polarization values, unless stated otherwise. The crustal residual polarizations (local anisotropy) vary laterally along the whole profile and are N160–190°E (yellow/orange colours in Fig. 7) in the section to the NW of the Jiangshan–Shaoxing fault (0–150 km), and N80–130°E (light blue/green colours in Fig. 7) along the section to the SE of this fault (150–380 km). These last polarization values demonstrate consistency with the *average* polarization direction, which is close to the N120°E direction that is the tectonic plate stress direction as deduced from the GPS measurements (Wang and Zhang 2001). The polarization directions of the faster split shear-waves also show variations in both the upper crust (above the depth of about 25 km) and the lower crust (within the depth range of 25 km to 35 km), although they are perhaps more visible in the southeast segment of the profile. Furthermore, the magnitude of shear-wave anisotropy as characterized by the time delays also varies along the profile from northwest to southeast, indicating the change in local anisotropy: the time delays are larger in the southeast than in the northwest. From the surface to the Moho, the time delays at shallow depths (less than 20 km) are also much higher than at deeper depths (in the lower crust).

4 Interpretations

4.1 Boundary between the Yangtze and the Cathaysia blocks

The Jiangshan–Shaoxing fault is geologically known to be of crustal scale (Hsu and Sun 1988; Hsu and Li 1990; Pei and Hong 1995; Gilder and Coe 1993, 1995; Gilder et al. 1996; Chen and John 1998; Hong et al. 1990, 2002), and is normally referred to as the boundary between the Yangtze and the Cathaysia blocks (Fig. 4), where the shear-wave velocity changes abruptly from 3.9 to 4.3 km/s at the top of the mantle (Zhang et al. 2005). The fast shear-wave polarizations of shear-wave splitting provide additional evidence to support this (Fig. 7). In the Yangtze block, northwest of the Jiangshan–Shaoxing fault, the polarizations are mainly in the north–south direction for the upper crust (shallower than 20 km). However, in the Cathaysia Block, to the southeast of the crust-scale fault, the polarizations of fast shear-waves are predominately in the N110–120°E direction, but other polarizations close to N90–100°E can be observed in other parts of the crust (Fig. 7).

4.2 Crustal deformation

Across major faults, there may be differences in geology and there may also be differences in maximum stress direction. Either or both of these differences can cause changes in polarization. Therefore, differences in the present local

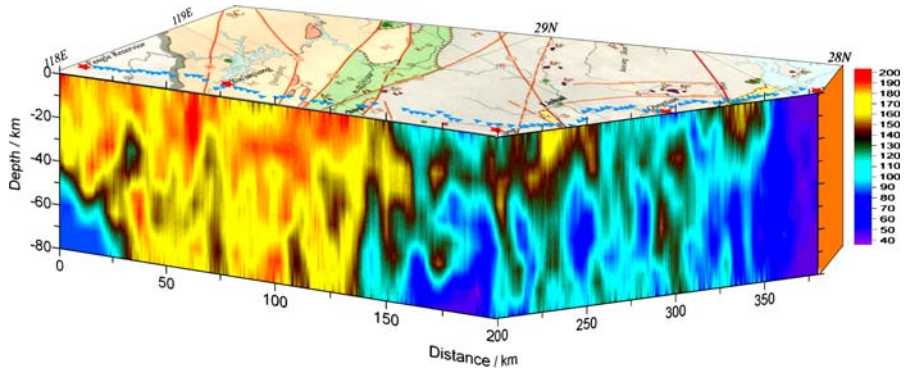

Fig. 7 Residual polarizations of fast split shear-wave as derived from shear-wave splitting parameters (Fig. 6). The *numbers* (and *colours*) represent residual polarizations in degrees East of North. Their lateral variations are consistent with faults crossed by the wide-angle seismic profile (*top of the plots*)

anisotropy across the faults may be the result of rocks with completely different formation histories being brought together, but not necessarily different stress directions. From the results of shear-wave splitting analysis as shown in Fig. 7, we find several polarization changes along the acquisition profile Tunxi–Wenzhou, and above all a conspicuous variation between the northwest and southeast transects at an offset of about 150 km which only provides further evidence for a deep lateral discontinuity which we recognize at the surface as a major fault (Jiangshan–Shaoxing).

Anyhow, even assuming that changes in local anisotropy across faults are as likely to be due to different geological histories, and different previous stress directions, rather than variations in the current stress direction, the split shear-wave polarization directions observed along the profile may indicate the directional variations of the plate movement, or the crustal deformations induced in the past by possible multi-stage collisions and thrusting. Because the polarization direction and the maximum stress direction coincide (Vinnik et al. 1989; Savage 1999), the force direction of the stress field has clearly changed on the two sides of the Jiangshan–Shaoxing fault belt and other regional faults along the section to the NW of the profile (Lin'an-Majin, Wuxing–Jiande, Qiuchuan–Xiaoshan and Quzhou–Tangxian) and the SE transect of the profile (Ningbo–Longquan and Zhenhai–Wenzhou). Therefore, the variation in both polarization and magnitude of local seismic anisotropy may indicate that the crust of the southeast of China endured multi-stage collisions as suggested by geologists (Hsu and Sun 1988; Hsu and Li 1990; Gilder and Coe 1993, 1995; Gilder et al. 1996; Pei and Hong 1995; Chen and John 1998). The above results are also consistent with the plate stress direction distribution from focal mechanism and fault plane solution (Xu and Wang 1986) and GPS measurements (Wang and Zhang 2001; Xu et al. 2002).

5 Conclusions

We have proposed a method to estimate the average of the shear-wave splitting parameters from wide-angle reflection seismic data. The synthetic and real data results demonstrate that the average time delay and polarization may be related to the regional stress field, whereas the residual anisotropy is attributed to local faulting. These results are potentially useful to understand the intralayer coupling/decoupling or deformation in the crust and upper mantle. Especially, the estimation of the local anisotropy from local fault activities may help to monitor the temporal activities of active faults if active source three-component measurements can be repeated in the specific earthquake occurrence zone and other interest areas (Gao and Crampin 2006).

Based on crustal shear-wave velocity model and seismic anisotropy analysis of the wide-angle seismic data in the southeast of China, we have obtained the polarization of fast shear-waves and magnitude of time-delay distribution between the fast and slow shear-waves. The results allow us to distinguish the Yangtze and the Cathaysia blocks with different orientation of polarizations and magnitude of seismic anisotropy in the corresponding crusts. Combining the crustal shear-wave velocity model, the velocity ratio of P- and S-waves, and the seismic anisotropy pattern, we support the argument that the Jiangshan–Shaoxing fault is the boundary between the Yangtze and the Cathaysia blocks (Zhang et al. 2000a, b, 2005, 2008). Through the analysis of the lateral variation of seismic anisotropy along the acquisition seismic profile Tunxi–Wenzhou, we find that there are four segments separated by the Lin'an–Majin fault, the Jiangshan–Shaoxing fault and the Zhenhai–Wenzhou fault with relatively constant seismic anisotropy, which may be attributed to early different stages of crustal deformations induced by the multi-stage collisions as suggested by Hsu and Sun (1988) and Hsu and Li (1990).

Acknowledgements The authors would like to thank Kun Liu, Bin Zhao, Xi Zhang and Yun Chen for their help with data processing and Institute of Geology and Geophysics, Chinese Academy of Sciences (CAS), for funding the data acquisition and the permission to publish this work, which is part of the aims stated in the Collaboration Agreement between the Institute of Geology and Geophysics and the University of Zaragoza, Spain. Dr. David Booth and other reviewers are especially appreciated for improvement of the manuscript. This work is supported by the Chinese Academy of Sciences with Grants KZCX2-109 and KZ951-B1-407, the National Natural Science Foundation of China with Grant 49825108 and the Ministry of Sciences and Technology of China.

References

Babuska V, Cara M (1991) Seismic anisotropy in the Earth. Kluwer, Dordrecht, The Netherlands

Booth DC, Crampin S (1985) Shear-wave polarizations on a curved wavefront at an isotropic free surface. Geophys J Int 83:31–45

Carbonell R, Smithson SB (1991) Crustal anisotropy and the structure of the Mohorovicic discontinuity in western Nevada of the basin and range province. In: RO Meissner et al (eds) Continental lithosphere, deep seismic reflections, Am. Geophys. Union, Washington, DC, pp 31–38

Chen JF, John BM (1998) Crustal evolution of southeastern China: Nd and Sr isotopic evidence. Tectonophysics 284:101–133

Christensen NI, Mooney WD (1995) Seismic velocity structure and composition of the continental crust: a global view. J Geophys Res 100:9761–9788

Crampin S, Gao Y (2006) A review of techniques for measuring seismic shear-wave splitting above small earthquakes. Phys Earth Planet Inter 159:1–14

Gao Y, Crampin S (2006) A further stress-forecast earthquake (with hindsight), where migration of source earthquakes causes anomalies in shear-wave polarizations. Tectonophysics 426(3–4):253–262

Gilder SA, Coe RS (1993) Cretaceous and Tertiary paleomagnetic results from Southeast China and their tectonic implications. Earth Planet Sci Lett 117: 637–652

Gilder SA, Coe RS (1995) Triassic paleomagnetic data from south China and their bearing on the tectonic evolution of the western circum-pacific region. Earth Planet Sci Lett 131:269–287

Gilder SA, Gill J, Coe RS (1996) Isotopic and paleomagnetic constraints on the Mesozoic tectonic evolution of south China. J Geophys Res 101:16137–16154

Godfrey NJ, Christensen NI, Okaya DA (2000) Anisotropy of schists: contribution of crustal anisotropy to active-source seismic experiments and shear-wave splitting observations. J Geophys Res 105:27991–28007

Hong D, Xie X, Zhang J (1990) Isotope geochemistry of granitoids in South China and their metallogeny. Res Geol 48:251–263

Hong D, Xie X, Zhang J (2002) Geological significance of the Hangzhou–Zhuguangshan–Huashan high granite belt. Geol Bull China 21:348–354

Hsu KJ, Sun S (1988) Mesozoic overthrust tectonics in South China. Geology 16:418–421

Hsu KJ, Li JL (1990) Tectonics of south China: key to understanding west Pacific geology. Tectonophysics 183:9–39

Huang C (1977) Basic features of the tectonic structure of China. Int Geol Rev 5:289–302

Kendall JM (2000) Seismic anisotropy in the boundary layers of the mantle. In: Karato S, Forte ARL, Master G, Strixrude L (eds) Earth's deep interior: mineral physics and tomography from the atomic to the global scale, Am. Geophys. Union.

Lafond CF, Levander A (1995) Migration of wide-aperture onshore–offshore seismic data, central California: seismic images of late stage subduction. J Geophys Res 100:22231–22244

Liu E, Crampin S (1990) Effects of internal shear-wave window: comparison with anisotropy-induced splitting. J Geophys Res 95:11,275–11,282

Mooney WD, Brocher TM (1987) Coincident seismic reflection/refraction studies of the continental lithosphere: a global review. Rev Geophys 25:723–742

Morozov IB, Levander A (2002) Depth image focusing in travel-time map based wide-angle migration. Geophysics 67:1903–1912

Pei R, Hong D (1995) The granites of south China and their metallogeny. Episodes 18:77–82

Savage MK (1999) Seismic anisotropy and mantle deformation: what have we learned from shear-wave splitting. Rev Geophys 37:65–105

Silver PG, Chan WW (1991) Shear-wave splitting for continental structure and evolution from seismic anisotropy. Nature 335:34–39

Teanby NA, Kendall JM (2004) Automation of shear-wave splitting measurements using cluster analysis. Bull Seismol Soc Am 94:453–463

Vecsey L, Plomerová J, Kozlovskaya E, Babuska V (2007) Shear-wave splitting as a diagnostic of variable anisotropic structure of the upper mantle beneath central Fennoscandia. Tectonophysics 438:57–77

Vinnik LP, Kind R, Makeyeva LI, Kosarev GL (1989) Azimuthal anisotropy in the lithosphere from observations of long-period S-waves. Geophys J Int 99:549–559

Wang Q, Zhang PZ (2001) Present-day crustal deformation in China constrained by global positioning system measurements. Science 294:574–577

Xiong S, Lai M, Liu H, Yu GS (1993) Lithosphere structure and velocity distribution from Tunxi to Wenzhou. In: Li J (ed) Lithosphere structure and geological evolution of Southeastern China. China Meteorological Press, Beijing

Xu Z, Wang S (1986) The state of stress field in continental China. Pure Appl Geophys 124:941–956

Xu JW, Zhu G, Tong WX (1987) Formation and evolution of the Tancheng–Lujiang wrench fault system: a major shear system to the northern of the Pacific Ocean. Tectonophysics 134:273–310

Xu CJ, Dong LX, Shi C (2002) A field of annual accumulation of strain energy density and its tectonic activity in North China by GPS measurements. Chinese J Geophys 45:517–526

Yang DH, Liu E, Zhang Z, Teng JW (2002) Finite-difference modelling in two-dimensional anisotropic media using a flux-corrected transport technique. Geophys J Int 148:320–328

Zhang ZM, Liou JG, Coleman RG (1984) An outline of the plate tectonics of China. Bull Geol Soc Am 95:295–312

Zhang Z, Li YK, Lu DY, Teng JW, Wang GJ (2000a) Velocity and anisotropy structure of the crust in the Dabieshan orogenic belt from wide-angle seismic data. Phys Earth Planet Inter 122:115–131

Zhang Z, Wang G, Teng J, Klemperer S (2000b) CDP mapping to obtain the fine structure of the crust and upper mantle from seismic sounding data: an example for the southeastern China. Phys Earth Planet Inter 122:133–146

Zhang Z, Badal J, Li Y, Chen Y, Yang LQ, Teng JW (2005) Crust–upper mantle seismic velocity structure across southeastern China. Tectonophysics 395:137–157

Zhang Z, Zhang X, Badal J (2008) Composition of the crust beneath southeastern China derived from an integrated geophysical dataset. J Geophys Res. 113 BO4417 doi:10.1029/2006JB004503

Zhou XM, Li WX (2000) Origin of late mesozoic igneous rocks in Southeastern China: implications for lithosphere subduction and underplating of mafic magmas. Tectonophysics 326:269–287